

# Overtone or higher harmonics? Prospects for testing the no-hair theorem with gravitational wave detections

Iara Ota\*

*Centro de Ciências Naturais e Humanas,  
Universidade Federal do ABC 09210-170 Santo André, SP, Brazil*

Cecilia Chirenti†

*Centro de Matemática, Computação e Cognição,  
Universidade Federal do ABC 09210-170 Santo André, SP, Brazil*

In light of the current (and future) gravitational wave detections, more sensitive tests of general relativity can be devised. Black hole spectroscopy has long been proposed as a way to test the no-hair theorem, that is, how closely an astrophysical black hole can be described by the Kerr geometry. We use numerical relativity simulations from the Simulating eXtreme Spacetimes project (SXS) to assess the detectability of one extra quasinormal mode in the ringdown of a binary black hole coalescence, with numbers  $(\ell, m, n)$  distinct from the fundamental quadrupolar mode  $(2, 2, 0)$ . Our approach uses the information from the complex waveform as well as from the time derivative of the phase in two different prescriptions that allow us to estimate the point at which the ringdown is best described by a single mode or by a sum of two modes. By scaling all amplitudes to a fiducial time  $t_{\text{peak}} + 10M$  ( $t_{\text{peak}}$  is the time of maximum waveform amplitude) our results for non-spinning binaries indicate that for mass ratios of 1:1 to approximately 5:1 the first overtone  $(2, 2, 1)$  will always have a larger excitation amplitude than the fundamental modes of the other harmonics  $(2, 1, 0)$ ,  $(3, 3, 0)$  and  $(4, 4, 0)$ , making it a more promising candidate for detection. In particular, for equal-mass binaries the ratio of the amplitude of the first overtone  $(2, 2, 1)$  to the fundamental mode  $(2, 2, 0)$  will be  $\gtrsim 0.65$ , whereas the corresponding ratio for the higher harmonics will be  $\lesssim 0.05$ . For binaries with mass ratios larger than 5:1 we find that the modes  $(2, 2, 1)$ ,  $(2, 1, 0)$  and  $(3, 3, 0)$  should have comparable amplitude ratios in the range  $0.3 - 0.4$ .

## I. INTRODUCTION

During their first two observing runs, O1 and O2, the LIGO-Virgo collaboration has detected gravitational waves (GWs) from ten binary black hole (BBH) mergers and one binary neutron star merger [1]. During the current observing run (O3), approximately one BBH merger is detected every week [2]. These detections represent an unparalleled feat of technological achievement and a triumph of general relativity (GR) (and of the numerical relativity (NR) simulations), with ongoing consequences for our understanding of astrophysics and fundamental physics. In particular, the current BBH mergers can potentially enable us to perform some long-sought tests of GR [3, 4].

In the ringdown phase after the merger, the GWs can be well approximated as a linear superposition of damped sinusoids, known as quasinormal modes (QNMs) (see [5] for a review). Their oscillation frequencies and damping times depend only on the properties of the final black hole. For each harmonic mode  $(\ell, m)$ , the waveform can

be expanded as a sum of overtones

$$\begin{aligned} \psi_{\ell m} &= \sum_n A_{\ell mn} e^{i[\omega_{\ell mn}(t-t_i) + \phi_{\ell mn}]} \\ &\equiv \sum_n \psi_{\ell mn}, \quad t \geq t_i, \end{aligned} \quad (1)$$

where the index  $n = 0, 1, 2, \dots$  labels the contribution of each overtone,  $A_{\ell mn}$  and  $\phi_{\ell mn}$  are respectively the initial amplitude and phase of each mode  $\psi_{\ell mn}$ ,  $\omega_{\ell mn} \equiv \omega_{\ell mn}^r + i\omega_{\ell mn}^i$  is the corresponding quasinormal mode complex frequency and  $t_i$  is the (unknown) starting time of the ringdown, usually expected to be after the time  $t_{\text{peak}}$  of maximum waveform amplitude.

The observation of two or more modes in a GW detection will allow us to test the no-hair theorem, as the oscillation frequencies and damping times of each mode should be uniquely determined by the mass and spin of the final black hole. This multi-mode analysis of the QNMs has been termed black hole spectroscopy [6–9] in analogy to standard electromagnetic spectroscopy, because the QNMs form the spectrum of the black hole.

The first GW event, GW150914 [10], showed that the fundamental quadrupolar mode - labeled as the  $(2, 2, 0)$  mode - can be detected in the signal, as long as the remnant black hole mass is such that its oscillation frequency is in the LIGO band (approximately 50–500 Hz). Most of the proposals for black hole spectroscopy focus on other fundamental harmonic modes  $(\ell, m, 0)$  and neglect the overtones of the quadrupolar mode,  $(2, 2, n)$  [11–15]. It is well known that the overtones decay much faster than

\* iara.ota@ufabc.edu.br

† cecilia.chirenti@ufabc.edu.br

the fundamental mode [5] and this has led to the expectation that their contribution could be neglected.<sup>1</sup>

However, this picture may be oversimplified. For example, it was shown in [19] that the addition of one overtone should increase the estimated signal to noise ratio (SNR) of a ringdown detection. Additionally, it was pointed out in [9] that the inclusion of overtones in the waveform should decrease the errors in the determination of the quadrupolar mode frequencies, mass and spin of the black hole remnant. More recently, it was suggested in [20] that with the inclusion of several overtones the gravitational waveform of a BBH merger can be described by a linear sum of QNMs starting at  $t_{\text{peak}}$ .

The observational situation is still unclear. A recent spectroscopic analysis of the GW150914 ringdown signal [21] found no evidence of the presence of more than one mode in the ringdown and showed that the modes (3, -3, 0), (3, -2, 0), (2, 1, 0) and (2, 2, 0) are all consistent with the remnant mass and spin found in the LIGO-Virgo analysis [22]. On the other hand, [23] re-analyzed the GW150914 data and found some evidence for the (2,2,1) mode. More recently [24] suggested that an SNR larger than  $\approx 30$  is necessary in order to perform black hole spectroscopy with overtones for nearly-equal mass BBH mergers.

Given the expected difficulties in detecting a second mode in the ringdown of a GW event, it will be useful to know *which mode* is most likely to be the second most relevant. Our goal is to compare the first overtone of the quadrupolar mode and the fundamental modes of the first higher harmonics to present the most promising case for a detection. One known source of ambiguity is that the excitation amplitudes of these exponentially damped modes depend on the chosen initial time for the ringdown.

Several methods for the determination of the starting time have been proposed (see for example [15, 25–27]), but most of them consider only the fundamental quadrupolar mode. Here we adapt existing techniques to estimate the contribution of the first overtone in the quadrupolar mode using the NR simulations from the Simulating eXtreme Spacetimes project (SXS) [28, 29]. For an event similar to GW150914 we expect  $R = A_{220}/A_{221} = 0.66$  (scaled at  $t_{\text{peak}} + 10M$ ), nearly 10 times larger than the contribution of the higher harmonics.

This paper is organized as follows: in Section II we fit a single mode to the ringdown to determine the parameters of the remnant black hole. In Section III we compute the initial time from which the ringdown of the quadrupolar mode is well described by the fundamental mode and

the first overtone, and the initial amplitude ratio of the two modes. In Section IV we generalize our results for increasing mass ratios and we find that the amplitude of the (2, 2, 1) mode will always be larger than or comparable to other harmonics. We present our closing remarks in Section V.

## II. DETERMINATION OF THE FUNDAMENTAL QNM

Throughout this section we will use the NR waveform SXS:BBH:0305, which is similar to the GW150914 detection [10, 30]. In the SXS simulations, the remnant mass  $M_f$  and dimensionless spin  $a$  are extracted from the apparent horizon [29] and, for this simulation, they are given in units of the total mass of the binary  $M = M_1 + M_2$  as  $M_f = 0.9520M$  and  $a = 0.6589M$ .

If the ringdown waveform  $\psi_{\ell m}$  (1) is fully described by the fundamental mode, that is,  $\psi_{\ell m} = \psi_{\ell m 0}$ , then the time derivative  $\dot{\theta}_{\ell m}$  of the complex phase defined as

$$\theta_{\ell m} \equiv \arctan \left[ \frac{\text{Im}(\psi_{\ell m})}{\text{Re}(\psi_{\ell m})} \right], \quad (2)$$

will be equal to the fundamental mode frequency of oscillation  $\omega_{\ell m 0}^r$ . However, the waveform  $\psi_{\ell m}$  has overtone contributions, as given by eq. (1), and  $\dot{\theta}_{\ell m}$  should not be simply constant and equal to  $\omega_{\ell m 0}^r$ . This can be seen for example in the recent work [31], where  $\dot{\theta}_{22}$  was computed in order to find a fitting formula for the final spin and it was found that  $\dot{\theta}_{22}$  is not constant in the interval  $t - t_{\text{peak}} \in [-20, 20]M$  (see Fig. 1 of [31]).

Nevertheless, the overtones decay much faster than the fundamental mode. In the particular case of the quadrupolar mode of the black hole remnant produced in the simulation SXS:BBH:0305, the damping times of the fundamental mode and the first overtone are  $\tau_{220} = 1/\omega_{220} = 11.9M$  and  $\tau_{221} = 1/\omega_{221} = 4.0M$ , respectively (see Table I). Therefore, if we assume that all modes are excited simultaneously, after some time  $t_{n=0}$  the contributions of all overtones will be negligible with respect to the fundamental mode and  $\dot{\theta}_{\ell m}(t \geq t_{n=0}) \approx \omega_{\ell m 0}^r$ .

Figure 1 shows in the upper plot  $\dot{\theta}_{22}$  in the ringdown of SXS:BBH:0305. For  $30M \lesssim t - t_{\text{peak}} \lesssim 75M$  we can see that  $\dot{\theta}_{22}$  approaches a constant value (with fractional variation less than approximately 1%), after the contributions of overtones or nonlinear effects from the merger have been damped away and before numerical errors introduce larger variations at late times. In this approximate interval we have fitted the fundamental mode strain

$$\psi_{220} = A_0 e^{-\omega_{220}^i t} [\cos(\omega_{220}^r t - \phi_0) + i \sin(\omega_{220}^r t - \phi_0)]$$

to the complex NR waveform shown in the lower plot, where  $A_0$ ,  $\phi_0$ ,  $\omega_{220}^r$  and  $\omega_{220}^i$  are free parameters in the fit. The frequencies obtained in this fit are  $M\omega_{220}^r = 0.5549$  and  $M\omega_{220}^i = 0.0848$ , and the mass and spin of the

<sup>1</sup> Even the detection of a single mode can allow for tests of some alternative theories of gravity (see for example [16]) and/or exotic models for compact objects in general relativity (see [17] for a review and [18] for an example of a direct test using the GW150914 data.)

final black hole computed from these frequencies [7, 32] are  $M_f = 0.9553M$  and  $a_f = 0.6632M$ . This means a correction of approximately 0.3% and 0.7% in the quoted mass and spin of the black hole remnant, respectively. The dashed horizontal line in the upper  $\dot{\theta}_{22}$  plot presents our best fit for  $\omega_{220}^r$ , which differs by approximately 0.2% from the value obtained with linear perturbation theory [7, 32, 33] and the quoted remnant mass and spin for this simulation, shown with the solid horizontal line.

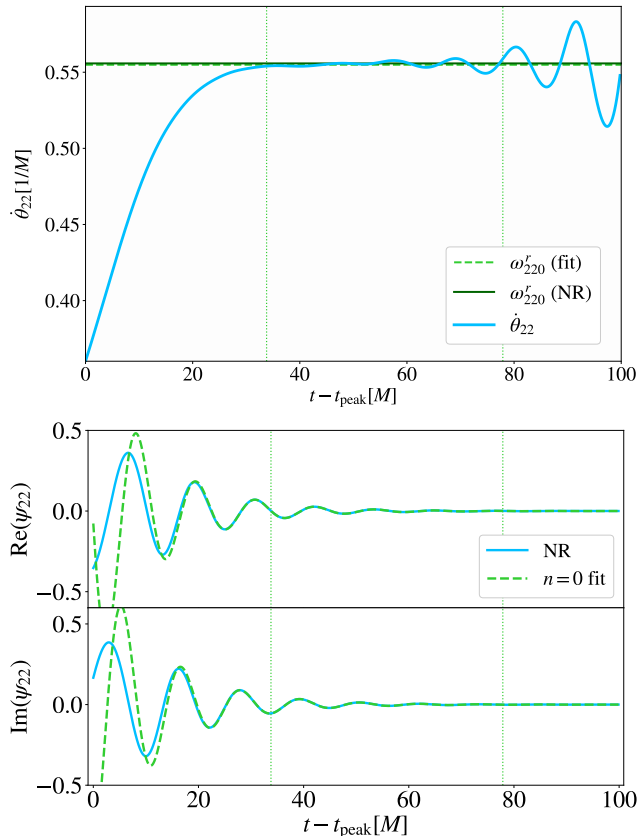


Figure 1. *Top*: Time derivative of the waveform phase  $\dot{\theta}_{22}$  in the ringdown of the binary black hole simulation SXS:BBH:0305. The solid horizontal line indicates the value of  $\omega_{220}^r$  obtained from the remnant parameters quoted in the NR simulation, while the (almost coincident) dashed line shows the value obtained by fitting the fundamental mode to the complex waveform (shown in the bottom plot) in the interval indicated by the dotted vertical lines. The oscillations at  $t - t_{\text{peak}} > 75M$  represent late time numerical errors. *Bottom*: The real and imaginary parts of the complex waveform (solid line) and the fundamental mode fit (dashed line).

We have also looked into the other harmonics (2,1), (3,3) and (4,4). Figure 2 reproduces the analysis presented in Figure 1, and again our results for frequencies  $\omega_{210}^r$ ,  $\omega_{330}^r$  and  $\omega_{440}^r$  agree with the corresponding values obtained with the previously quoted parameters within less than approximately 0.2%. These  $\dot{\theta}_{\ell m}$  also rise from lower values towards  $\omega_{\ell m 0}^r$  when the overtones and possible non-linear behavior have been damped. Numerical

errors become more relevant at later times.

Table I. Fundamental and first overtone quasinormal mode frequencies of the quadrupolar  $(\ell, m) = (2, 2)$  mode for a black hole remnant with parameters  $M_f = 0.9553M$  and  $a = 0.6632M$ , inferred from SXS:BBH:0305.

$n$	$M\omega_{22n}^r$	$M\omega_{22n}^i$
0	0.5549	0.0848
1	0.5427	0.2564

### III. IMPROVED RINGDOWN: FUNDAMENTAL MODE + FIRST OVERTONE

It is clear from Figures 1 and 2 that the waveform immediately after the amplitude peak is not fully described by the fundamental mode, as in that case we would have a constant  $\dot{\theta}_{\ell m} = \omega_{\ell m 0}^r$ . The observed variation can be associated with a non-linear behavior near the peak or non-negligible contributions of overtones. The presence of the overtones can be made evident by subtracting the lowest order modes from the signal (see Fig. 7 in [34] for an example of this approach). In [20] it was suggested that, by including seven overtones in the model, the linear behavior of the waveform starts at the peak of the amplitude (or even before the peak).

However, given the expected difficulties in observing and identifying other modes besides the fundamental quadrupolar mode in the gravitational wave data [21, 23, 30], here we will only consider the contribution of the first overtone in the signal. We will do this by fitting to the numerical data functions containing the fundamental mode and the first overtone with frequencies given by Table I and we will determine the interval of the waveform which is well described by *the fundamental mode and the first overtone*<sup>2</sup>.

To determine the initial time of this interval, we will use two methods. In the first method we perform a non-linear fit to the numerical waveform  $\psi_{22}$  of the 4-parameter function

$$\begin{aligned} \psi_{22}(t) = & A_{220} e^{-\omega_{220}^i t} [\cos(\omega_{220}^r t - \phi_{220}) + \\ & + i \sin(\omega_{220}^r t - \phi_{220})] \\ & + A_{221} e^{-\omega_{221}^i t} [\cos(\omega_{221}^r t - \phi_{221}) + \\ & + i \sin(\omega_{221}^r t - \phi_{221})], \end{aligned} \quad (3)$$

where  $\omega_{22i}^{(r,i)}$  are given by Table I, and the fitting parameters are the initial amplitudes  $A_{22i}$  and the initial phases

<sup>2</sup> It is important to notice that the initial times we obtained do not necessarily represent the beginning of the post-merger linear regime (i.e., the ringdown) as non-negligible contributions of higher overtones ( $n \geq 2$ ) in the waveform are not taken into account.

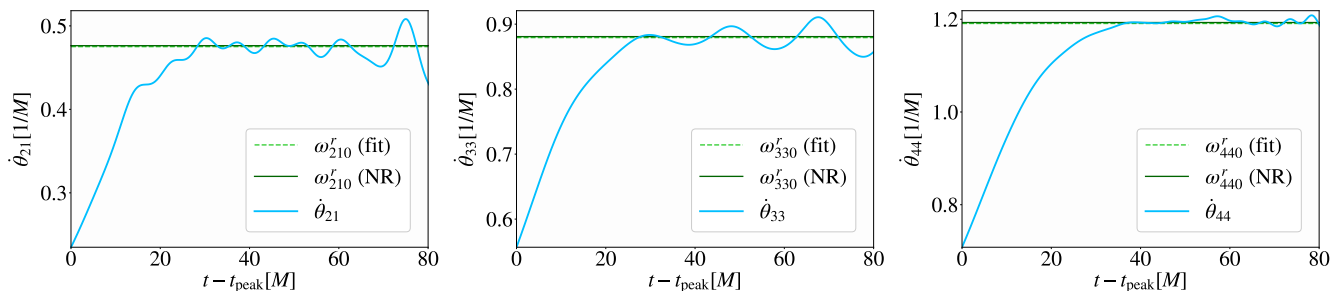


Figure 2. Same as the upper plot of Figure 1, but for the time derivative of the waveform phases  $\theta_{21}$  (left),  $\theta_{33}$  (middle) and  $\theta_{44}$  (right). Again we see that there is very good agreement (less than 0.2% difference) between the values of  $\omega_{\ell m 0}^r$  obtained from the remnant parameters quoted in the NR simulation and our fitted values.  $\dot{\theta}_{\ell m}$  approaches  $\omega_{\ell m 0}^r$  after the overtone contributions and non-linearities have decayed (and before the late time numerical errors become too relevant).

$\phi_{22i}$  of each mode ( $i = 0, 1$ ). In our second method we do a non-linear fit to the numerical  $\theta_{22}$  of the 2-parameter function

$$\begin{aligned} \dot{\theta}_{22}(t) = & \left\{ \omega_{220}^r + R^2 e^{2(\omega_{220}^i - \omega_{221}^i)t} \omega_{221}^r + R e^{(\omega_{220}^i - \omega_{221}^i)t} \right. \\ & \times [(\omega_{220}^r + \omega_{221}^r) \cos((\omega_{220}^r - \omega_{221}^r)t - \phi) \\ & \left. + (\omega_{221}^i - \omega_{220}^i) \sin((\omega_{220}^r - \omega_{221}^r)t - \phi)] \right\} \\ & \times \left[ 2R e^{(\omega_{220}^i - \omega_{221}^i)t} \cos((\omega_{220}^r - \omega_{221}^r)t - \phi) \right. \\ & \left. + R^2 e^{2(\omega_{220}^i - \omega_{221}^i)t} + 1 \right]^{-1}, \end{aligned} \quad (4)$$

where the fitting parameters are the ratio of the initial amplitudes  $R \equiv A_{221}/A_{220}$  and the phase difference between the modes  $\phi \equiv \phi_0 - \phi_1$ . Since  $\omega_{221}^i > \omega_{220}^i$ , we have that  $e^{(\omega_{220}^i - \omega_{221}^i)t} \rightarrow 0$  and  $\dot{\theta}_{22} \rightarrow \omega_{220}^r$  as  $t \rightarrow \infty$ .

The initial time  $t_0$  for the fits (3) and (4) is not treated as a fitting parameter. We select the best initial time  $t_0$  by minimizing the mismatch  $\mathcal{M}$  between the NR data  $f_{\text{NR}}$  and the fitted function  $f_{\text{fit}}$ , defined as

$$\mathcal{M} = 1 - \frac{\langle f_{\text{NR}}, f_{\text{fit}} \rangle}{\sqrt{\langle f_{\text{NR}}, f_{\text{NR}} \rangle \langle f_{\text{fit}}, f_{\text{fit}} \rangle}}. \quad (5)$$

where  $f$  represents either the waveform  $\psi_{22}$  or the phase derivative  $\theta_{22}$ . The mismatch  $\mathcal{M}$  is a function of the initial time  $t_0$ , as the inner products in the right-hand side are computed starting at each  $t_0$ . This procedure is similar to the one used in [20]. Other approaches suggested in the literature for finding the initial time of the ringdown minimize the residuals of the fit of the fundamental mode, see for example [15, 25, 26].

Following [35], the inner product can be defined in the usual way:

$$\langle \psi, \varphi \rangle_{\text{standard}} \equiv \left| \int_{t_0} \psi^* \varphi dt \right|, \quad (6)$$

where the star denotes the complex conjugate. However, QNMs are not orthogonal and complete with respect to the inner product defined above, which presents a problem for computing how much energy is contained in each

mode. To circumvent this problem, Nollert [35, 36] suggested an energy-oriented inner product defined as

$$\langle \psi, \varphi \rangle_{\text{energy}} \equiv \left| \int_{t_0} \dot{\psi}^* \dot{\varphi} dt \right|, \quad (7)$$

where the dot denotes the time derivative as before. We will use both of the inner product definitions (6) and (7) in our calculation of the mismatch (5). The mismatch will be calculated for the fits (3) and (4), giving four estimates for the time  $t_0$ , as we will see below.

Again, here we will not determine the initial time of the ringdown stage but the initial time  $t_0$  at which the waveform is well described by the sum of the fundamental mode and the first overtone. Figure 3 shows the mismatch of the simulation SXS:BBH:0305 as a function of the initial time for the phase derivative  $\dot{\theta}_{22}$  (black) and for the waveform  $\psi_{22}$  (red). Solid (dashed) lines indicate that the inner product was calculated with eq. (6) (eq. (7)). We choose the initial time  $t_0$  as the first minimum of the mismatch  $\mathcal{M}$ , ignoring the local minima in the oscillations when  $\mathcal{M}$  is still decreasing. The highlighted points (blue crosses and gray dots) in Figure 3 show the initial time for each of the four calculations.

The initial time  $t_0$  depends on the method (choice of inner product and fitting function). The dashed black curve shows a clear minimum at about  $t_0 - t_{\text{peak}} = 10M$  (marked with a blue cross), and the largest values for the mismatch (because  $\dot{\theta}_{22} \approx 0$  for  $\theta_{22} \approx \omega_{220}^r$ ). The solid black curve shows that the mismatch stops decreasing at approximately that time, but the actual first minimum is marked by the gray dot and it is typically less precisely determined because of the flattening of the curve. The dashed and solid red curves show very similar behaviors, with a minimum close to  $t_0 - t_{\text{peak}} = 15.6M$  (blue cross) but the dashed curve presents more oscillations and local minima that make the determination of  $t_0$  more uncertain (gray dot).

With these general considerations, which are typical of all simulations we have analyzed, we have chosen to keep the estimates for  $t_0$  given by only two methods, which look for:

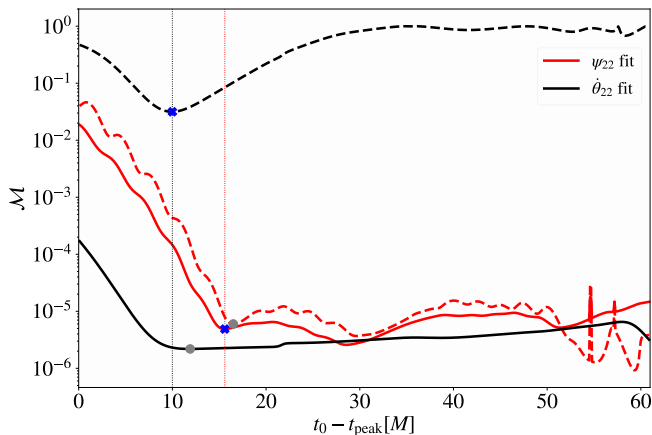


Figure 3. Mismatch (5) between simulation SXS:BBH:0305 and a ringdown model with two modes (fundamental quadrupole + first overtone) as a function of time. The mismatch is calculated for the complex waveform  $\psi_{22}$  (3) in red and for the phase derivative  $\dot{\theta}_{22}$  (4) in black. Solid (dashed) lines indicate that the inner product is calculated using eq. (6) (eq. (7)). The points show the chosen initial time  $t_0$  for each case. The round gray points will not be considered in our analysis and the blue crosses are the chosen initial times for each function:  $\dot{\theta}_{22}$  (method I) and  $\psi_{22}$  (method II) (see text).

I the minimum of the mismatch of  $\dot{\theta}_{22}$  computed with the energy-oriented inner product given by eq. (7)

II the first minimum of the mismatch of  $\psi_{22}$  computed with the standard inner product given by eq. (6),

which are shown in Figure 3 with blue crosses on the dashed black and solid red curves, respectively.

Our results are compatible with the recent multimode analysis of the ringdown phase of the GW150914 detection [21], where the initial time is defined as the time in which the fundamental mode (of both  $\ell = 2$  and  $\ell = 3$ ) has the highest probability of matching the data. These estimates also agree with the time at which the frequency and damping time of the fundamental quadrupolar mode match values obtained from the data analysis of GW150914 [8, 30].

Figure 4 shows in the two upper plots the values obtained with our two different fits for the the initial amplitude ratio  $R$  (left) and initial phase difference  $\phi$  (right) as a function of the initial time  $t_0$ . The dotted vertical lines show again the best initial times obtained from methods I and II, see Figure 3. Both  $\phi$  and  $R$  decrease with the initial time  $t_0$ , but we note that method I is more sensitive and presents unphysical variations after the best initial time as  $R$  approaches zero (and consequently  $\dot{\theta}_{22} \rightarrow 0$ ). A similar behavior is also present for  $\phi$  obtained with method II at slightly later times, not shown in the plot.

Even if our estimates for the initial time  $t_0$  do not coincide with the initial time of the ringdown, we expect that the amplitude ratio calculated at  $t_0^\alpha$  (where  $\alpha = \text{I, II}$  labels the method used) should be correct even if the

ringdown starts before  $t_0^\alpha$ . As long as the linear regime is valid, the amplitude ratio as a function of time can be written as

$$\mathcal{R}^\alpha(t) = R^\alpha(t_0^\alpha) e^{(\omega_{221}^i - \omega_{220}^i)(t_0^\alpha - (t - t_{\text{peak}}))}, \quad (8)$$

where  $R^\alpha(t_0^\alpha)$  is the fitted amplitude ratio  $R^\alpha$  at the best initial time  $t_0^\alpha$  for each fit. Similarly, we can also write the phase difference as a function of time

$$\varphi^\alpha(t) = \phi^\alpha(t_0^\alpha) - (\omega_{220}^r - \omega_{221}^i)(t - t_0^\alpha). \quad (9)$$

Expressions (8) and (9) are also represented in the upper plots of Figure 4 as dotted curves. Our results show very good agreement for  $R$  between the two methods around the best initial times  $t_0^\alpha$ , with larger deviations observed for  $\phi$ . In the lower plots, the relative difference between the fits and the expressions for  $\mathcal{R}^\alpha$  and  $\varphi^\alpha$  is shown as a function of time. In both plots the larger differences at earlier times indicate that near  $t_{\text{peak}}$  the non-linear dynamics or the higher overtones have significant contributions in the waveform, while the larger differences at later times are caused by the exponential vanishing of  $R$ .

Finally, in Figure 5 we present a comparison between the simulation SXS:BBH:0301 (solid blue) and our best fits for the fundamental model and for the fundamental mode + first overtone. The fits are performed at the best initial times ( $t_{n=0}$ ,  $t_0^{\text{I}}$  and  $t_0^{\text{II}}$ ) shown with vertical lines. Both for the waveform  $\psi_{22}$  and for the phase derivative  $\dot{\theta}_{22}$  we can see that adding the first overtone pushes back the best initial time for the fit, but the residuals are comparable after  $t_{n=0}$ .

In summary, we have found out that the waveform has a non negligible contribution from the first overtone, with an amplitude ratio  $R = A_{221}/A_{220} = 0.66$  at  $t_0^{\text{I}} = t_{\text{peak}} + 10M$ . So far, most spectroscopic analyses have neglected the overtones and focused instead on higher harmonic modes. However, higher harmonic modes have very low excitation amplitudes relative to the quadrupolar mode. In the example we have considered so far, we have found that the amplitude ratios corresponding to the next higher harmonics are  $A_{210}/A_{220} = 0.05$ ,  $A_{330}/A_{220} = 0.07$ ,  $A_{440}/A_{220} = 0.04$ . Therefore, detections of higher harmonic modes should not be expected in the LIGO/Virgo data. However, the first overtone seems to have an excitation amplitude high enough to be seen in data analyses of the ringdown phase, as indicated by the preliminary work done in [23].

#### IV. MASS RATIO DEPENDENCE

Now we will systematically explore SXS simulations with increasing mass ratio  $q \equiv M_1/M_2$  and initial zero-spin, in order to assess how relevant a contribution the first overtone will have in binary black hole systems with non-equal mass ratios.

We have reproduced our analysis for a set of 19 simulations with  $q$  ranging from 1 to 10. The upper left

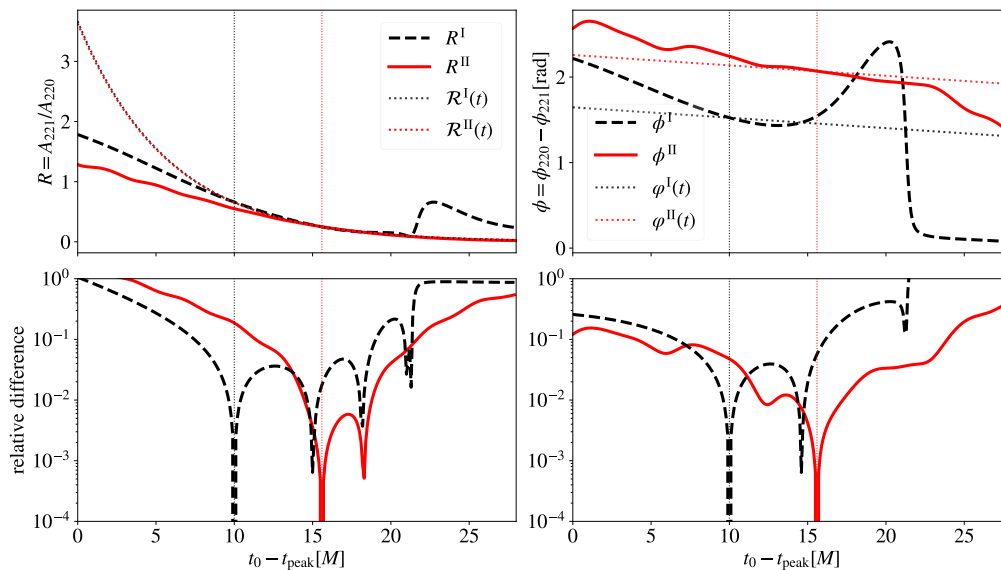


Figure 4. *Top left*: Amplitude ratio  $R^\alpha = A_{221}/A_{220}$  between the first overtone and the fundamental mode as a function of the initial time, where  $\alpha$  labels methods I and II as defined in Figure 3 and in the text. The dotted curves show the expected time-dependence in the linear regime  $\mathcal{R}^\alpha(t)$  (8) adjusted to the best initial times  $t_0^\alpha$  as obtained in Figure 3, indicated with vertical lines. *Bottom left*: Relative difference between the fitted ratio  $R^\alpha$  and the expected time-dependent ratio  $\mathcal{R}^\alpha$ . The increasing difference between  $R^\alpha$  and  $\mathcal{R}^\alpha$  towards  $t_{\text{peak}}$  may be due to non-negligible contributions of higher overtones or non-linear dynamics in the waveform, while the increasing errors for larger  $t$  come from the vanishing of  $R^\alpha$  at later times. *Top and bottom right*: Same as in the left panels, but for the phase difference  $\phi^\alpha = \phi_{220} - \phi_{221}$  between the first overtone and the fundamental mode and the expected time dependence in the linear regime  $\varphi^\alpha(t)$  (9).

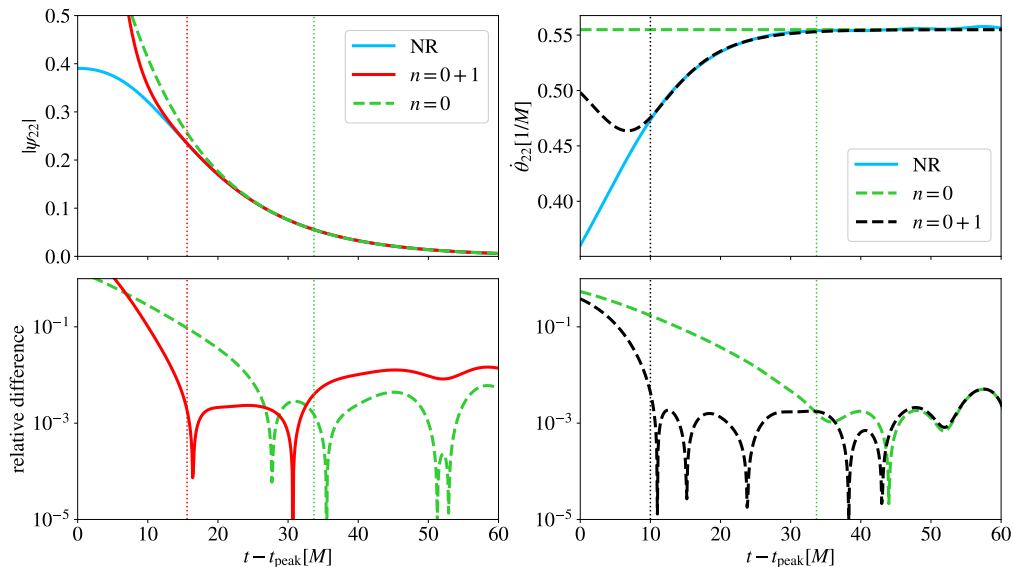


Figure 5. *Top*: Amplitude of the ringdown waveform  $|\psi_{22}|$  (left) and time derivative of the phase  $\dot{\theta}_{22}$  (right) as a function of time (right) for the SXS:BBH:0305 NR simulation, together with our best fits for the ringdown considering only the fundamental mode ( $n = 0$ ) and the fundamental mode + first overtone ( $n = 0 + 1$ ), using the best initial times  $t_0^\alpha$  found with methods I (right) and II (left). *Bottom*: Relative differences between the fits and the simulation as a function of time. The dotted vertical lines indicates the initial times for each fit, as shown before in Figures 1 and 3.

plot in Figure 6 shows the initial time  $t_0$  as a function of the binary mass ratio  $q$ . We can see that the waveform is well described by the fundamental mode and the first

overtone at earlier times for higher mass ratios: as the binary mass ratio increases, the linear perturbation regime is approached closer to the merger and the contributions

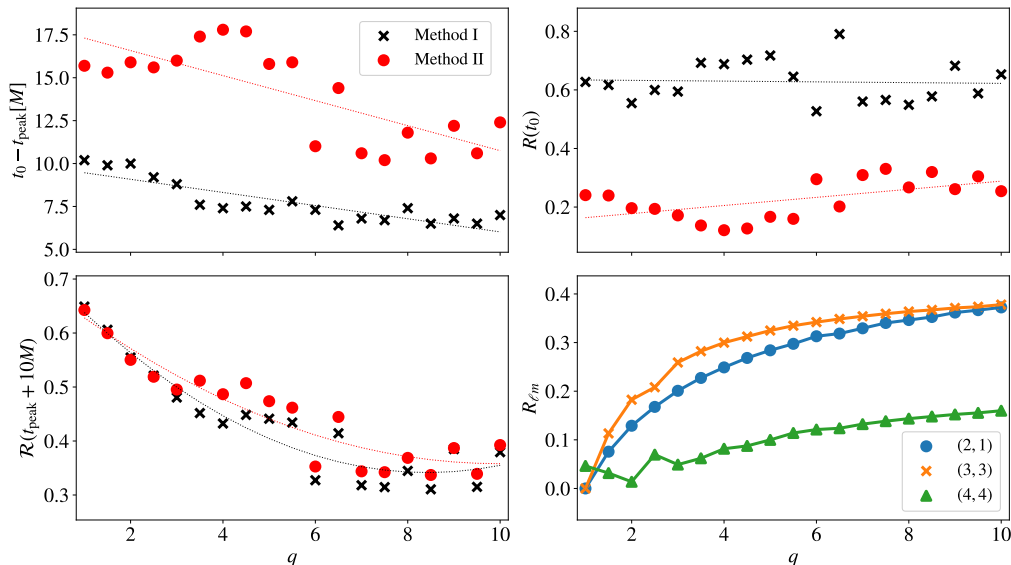


Figure 6. *Top*: Initial times  $t_0$  (left) and amplitude ratio  $R = A_{221}/A_{220}$  determined at  $t_0$  (right) as a function of the binary mass ratio  $q$ , obtained with methods I and II (defined in Figure 3). The ringdown waveform is well described by the fundamental mode and the first overtone at earlier times for higher mass ratios. *Bottom*: Amplitude ratio  $\mathcal{R}(t)$  as defined before (left) and amplitude ratio  $R_{\ell m} = A_{\ell m 0}/A_{220}$  between the fundamental mode of the higher harmonic modes  $(\ell, m) = (2, 1)$ ,  $(3, 3)$  and  $(4, 4)$  and the fundamental quadrupolar mode  $(2, 2)$ , both evaluated at  $t = t_{\text{peak}} + 10M$ , as a function of the mass ratio. Methods I and II show good agreement, once corrected to the same fiducial time.  $R_{\ell m}$  is approximately independent of the initial time. The first overtone has a higher amplitude than all harmonic mode for lower mass ratios ( $q \lesssim 5$ ) and is comparable to the modes  $(2, 1)$  and  $(3, 3)$  for higher mass ratios.

of the overtones become less relevant.

In the upper right plot of Figure 6 we present the amplitude ratio  $R$  at  $t_0$  as a function of the binary mass ratio  $q$ . The observed spread is mostly explained by the dependence of  $t_0$  on  $q$ , and the results obtained with both methods can be nicely unified when we present the expected values obtained with eq. (8) at the same fiducial time  $t = t_{\text{peak}} + 10M$  in the lower left plot.

The lower right plot of Figure 6 shows the amplitude ratio  $R_{\ell m}$  between the fundamental mode of the higher harmonic modes  $(\ell, m) = (2, 1)$ ,  $(3, 3)$  and  $(4, 4)$  and the fundamental quadrupolar mode  $(2, 2)$  at  $t = t_{\text{peak}} + 10M$ . We can see that the first overtone  $(2, 2, 1)$  has a higher amplitude ratio  $R$  than all harmonic modes for lower mass ratios  $q \lesssim 5$ . For higher mass ratios,  $R$  seems to asymptote to a constant and it is comparable to the  $(2, 1, 0)$  and  $(3, 3, 0)$  values. We also note that  $R_{\ell m}$  does not depend on the initial time due to similar damping times between the fundamental modes with different  $(\ell, m)$  (see Table II), and that our results for the higher harmonics are in good agreement with those of Fig. 1 of [11].

## V. CONCLUSIONS

We have used NR simulations from the Simulating extreme Spacetimes project (SXS) [28, 29] to estimate the contribution of overtones and higher harmonics in the ringdown of a BBH merger, with the aim to identify

Table II. Ringdown frequencies of the fundamental mode for the first harmonics of a remnant black hole with mass  $M_f = 0.9540M$  and final spin  $a = 0.6556M$ , resulting from the merger of an equal mass ( $q = 1$ ) non-spinning binary.

$(\ell, m, n)$	$M\omega_{\ell mn}^r$	$M\omega_{\ell mn}^i$
$(2, 2, 0)$	0.5524	0.0852
$(2, 1, 0)$	0.4742	0.0865
$(3, 3, 0)$	0.8757	0.0874
$(4, 4, 0)$	1.1861	0.0889

the most promising route for observationally testing the no-hair theorem using gravitational wave detections and black hole spectroscopy.

Initially we focused on the quadrupolar mode and we used the waveform  $\psi_{22}$  and the time derivative of the phase  $\theta_{22}$  in two different methods to determine the initial time  $t_0$  from which the simulated data is well described by the  $(2, 2, 0)$  and the  $(2, 2, 1)$  modes. For the nearly-equal mass case we found a initial time in agreement with previous ringdown analyses [15, 21, 27]. Additionally, we found that the initial times obtained decrease with increasing mass ratio of the binary system.

By scaling the excitation amplitudes to a fiducial time  $t_{\text{peak}} + 10M$  we found that the  $(2, 2, 1)$  mode will always be more significant than the fundamental higher harmonic modes for BBH systems with low mass ratios, from 1:1

to approximately 5:1. In particular, for equal masses we have  $R = A_{221}/A_{220} = 0.66$ , more than 10 times larger than the amplitudes of the other harmonics. For mass ratios larger than 5:1, our results indicate an interesting “equipartition” and the (2,2,1), (2,1,0) and (3,3,0) modes have comparable amplitudes of approximately  $0.35A_{220}$ .

All of the GW detections reported so far are compatible with equal-mass black hole binaries [1, 37, 38]. Therefore our results indicate a promising prospect for using the GW data to test the no-hair theorem with overtones, even though it is expected that in O3 and future observing runs some events with a higher mass ratio may also be detected.

However, the close frequencies of the (2,2,0) and (2,2,1) modes and the faster damping time of the overtone will necessarily make this a challenging detection. A coherent mode stacking analysis [39, 40] may be needed to improve the significance of the first overtone in a Bayesian model comparison, which we expect to perform with the already reported detections. We are also working on extending our analysis to cases with non-zero initial spins and eccentricities (we considered here only one case with nonzero spins in Sections II and III), as it is well known that initial spin affects the higher harmonics excitation amplitudes [11].

It is likely that a positive (and accurate) identification of the (2,2,1) mode in the GW data will have to wait for more signals with higher SNR. However, this

is only a matter of time, and the development of the necessary analysis tools and theoretical understanding is timely. We need to be prepared for the surprises that will undoubtedly come from GW astronomy.

## ACKNOWLEDGMENTS

We thank Vitor Cardoso, Max Isi, Luis Lehner, Cole Miller, Luciano Rezzolla and Erik Schnetter for useful discussions and comments on our work. We are especially thankful to Bernard Kelly for his help in the initial stages of this project. IO was partially supported by grant 2018/21286-3 of the São Paulo Research Foundation (FAPESP) and by the Federal University of ABC. CC acknowledges support from grant 303750/2017-0 of the Brazilian National Council for Scientific and Technological Development (CNPq). We are grateful for the hospitality of Perimeter Institute where part of this work was carried out. Research at Perimeter Institute is supported in part by the Government of Canada through the Department of Innovation, Science and Economic Development Canada and by the Province of Ontario through the Ministry of Economic Development, Job Creation and Trade. This research was also supported in part by the Simons Foundation through the Simons Foundation Emmy Noether Fellows Program at Perimeter Institute.

- 
- [1] B. P. Abbott *et al.* (LIGO Scientific, Virgo), *Phys. Rev.* **X9**, 031040 (2019), arXiv:1811.12907 [astro-ph.HE].
  - [2] <https://gracedb.ligo.org/>.
  - [3] N. Yunes and X. Siemens, *Living Rev. Rel.* **16**, 9 (2013), arXiv:1304.3473 [gr-qc].
  - [4] L. Barack *et al.*, *Classical and Quantum Gravity* **36**, 143001 (2019).
  - [5] K. D. Kokkotas and B. G. Schmidt, *Living Rev. Rel.* **2**, 2 (1999), arXiv:gr-qc/9909058 [gr-qc].
  - [6] O. Dreyer, B. J. Kelly, B. Krishnan, L. S. Finn, D. Garrison, and R. Lopez-Aleman, *Class. Quant. Grav.* **21**, 787 (2004), arXiv:gr-qc/0309007 [gr-qc].
  - [7] E. Berti, V. Cardoso, and C. M. Will, *Phys. Rev.* **D73**, 064030 (2006), arXiv:gr-qc/0512160 [gr-qc].
  - [8] R. Brito, A. Buonanno, and V. Raymond, *Phys. Rev.* **D98**, 084038 (2018), arXiv:1805.00293 [gr-qc].
  - [9] V. Baibhav, E. Berti, V. Cardoso, and G. Khanna, *Phys. Rev.* **D97**, 044048 (2018), arXiv:1710.02156 [gr-qc].
  - [10] B. P. Abbott *et al.* (LIGO Scientific, Virgo), *Phys. Rev. Lett.* **116**, 061102 (2016), arXiv:1602.03837 [gr-qc].
  - [11] R. Cotesta, A. Buonanno, A. Bohé, A. Taracchini, I. Hinder, and S. Ossokine, *Phys. Rev.* **D98**, 084028 (2018), arXiv:1803.10701 [gr-qc].
  - [12] I. Kamaretsos, M. Hannam, S. Husa, and B. S. Sathyaprakash, *Phys. Rev.* **D85**, 024018 (2012), arXiv:1107.0854 [gr-qc].
  - [13] B. J. Kelly and J. G. Baker, *Phys. Rev.* **D87**, 084004 (2013), arXiv:1212.5553 [gr-qc].
  - [14] C. Shi, J. Bao, H. Wang, J.-d. Zhang, Y. Hu, A. Sesana, E. Barausse, J. Mei, and J. Luo, *Phys. Rev.* **D100**, 044036 (2019), arXiv:1902.08922 [gr-qc].
  - [15] E. Thrane, P. D. Lasky, and Y. Levin, *Phys. Rev.* **D96**, 102004 (2017), arXiv:1706.05152 [gr-qc].
  - [16] V. Cardoso, M. Kimura, A. Maselli, E. Berti, C. F. Macedo, and R. McManus, *Physical Review D* **99** (2019), 10.1103/physrevd.99.104077.
  - [17] V. Cardoso and P. Pani, *Living Rev. Rel.* **22**, 4 (2019), arXiv:1904.05363 [gr-qc].
  - [18] C. Chirenti and L. Rezzolla, *Phys. Rev.* **D94**, 084016 (2016), arXiv:1602.08759 [gr-qc].
  - [19] L. London, D. Shoemaker, and J. Healy, *Phys. Rev.* **D90**, 124032 (2014), [Erratum: *Phys. Rev.D94,no.6,069902(2016)*], arXiv:1404.3197 [gr-qc].
  - [20] M. Giesler, M. Isi, M. Scheel, and S. Teukolsky, (2019), arXiv:1903.08284 [gr-qc].
  - [21] G. Carullo, W. Del Pozzo, and J. Veitch, *Phys. Rev.* **D99**, 123029 (2019), arXiv:1902.07527 [gr-qc].
  - [22] B. P. Abbott *et al.* (LIGO Scientific, Virgo), *Phys. Rev. Lett.* **116**, 241102 (2016), arXiv:1602.03840 [gr-qc].
  - [23] M. Isi, M. Giesler, W. M. Farr, M. A. Scheel, and S. A. Teukolsky, *Phys. Rev. Lett.* **123**, 111102 (2019), arXiv:1905.00869 [gr-qc].
  - [24] S. Bhagwat, X. J. Forteza, P. Pani, and V. Ferrari, (2019), arXiv:1910.08708 [gr-qc].
  - [25] E. N. Dorband, E. Berti, P. Diener, E. Schnetter, and M. Tiglio, *Phys. Rev.* **D74**, 084028 (2006), arXiv:gr-qc/0608091 [gr-qc].
  - [26] E. Berti, V. Cardoso, J. A. Gonzalez, U. Sperhake,

- M. Hannam, S. Husa, and B. Bruegmann, *Phys. Rev. D* **76**, 064034 (2007), arXiv:gr-qc/0703053 [GR-QC].
- [27] G. Carullo *et al.*, *Phys. Rev. D* **98**, 104020 (2018), arXiv:1805.04760 [gr-qc].
- [28] M. Boyle *et al.*, *Class. Quant. Grav.* **36**, 195006 (2019), arXiv:1904.04831 [gr-qc].
- [29] <https://data.black-holes.org/waveforms/index.html>.
- [30] B. P. Abbott *et al.* (LIGO Scientific, Virgo), *Phys. Rev. Lett.* **116**, 221101 (2016), [Erratum: *Phys. Rev. Lett.* 121,no.12,129902(2018)], arXiv:1602.03841 [gr-qc].
- [31] D. Ferguson, S. Ghonge, J. A. Clark, J. C. Bustillo, P. Laguna, and D. Shoemaker, (2019), arXiv:1905.03756 [gr-qc].
- [32] <https://pages.jh.edu/~eberti2/ringdown/>.
- [33] E. Berti and V. Cardoso, *Phys. Rev. D* **74**, 104020 (2006), arXiv:gr-qc/0605118 [gr-qc].
- [34] C. B. M. H. Chirenti and L. Rezzolla, *Classical and Quantum Gravity* **24**, 4191–4206 (2007).
- [35] H.-P. Nollert, *The Eighth Marcel Grossmann Meeting* (World Scientific Pub Co Inc, 1999).
- [36] H.-P. Nollert, *Class. Quant. Grav.* **16**, R159 (1999).
- [37] T. Venumadhav, B. Zackay, J. Roulet, L. Dai, and M. Zaldarriaga, (2019), arXiv:1904.07214 [astro-ph.HE].
- [38] B. Zackay, L. Dai, T. Venumadhav, J. Roulet, and M. Zaldarriaga, (2019), arXiv:1910.09528 [astro-ph.HE].
- [39] H. Yang, K. Yagi, J. Blackman, L. Lehner, V. Paschalidis, F. Pretorius, and N. Yunes, *Physical Review Letters* **118** (2017), 10.1103/physrevlett.118.161101.
- [40] E. Berti, K. Yagi, H. Yang, and N. Yunes, *General Relativity and Gravitation* **50** (2018), 10.1007/s10714-018-2372-6.